Journal of Coordination Chemistry

ISSN: 0095-8972 (Print) 1029-0389 (Online) Journal homepage: http://www.tandfonline.com/loi/gcoo20

Enabling visible-light water photooxidation by coordinative incorporation of Co(II/III) cocatalytic sites into organic-inorganic hybrids: quantum chemical modeling and photoelectrochemical performance

Oleksiy V. Khavryuchenko, Lidong Wang, Dariusz Mitoraj, Gilles H. Peslherbe & Radim Beranek

To cite this article: Oleksiy V. Khavryuchenko, Lidong Wang, Dariusz Mitoraj, Gilles H. Peslherbe & Radim Beranek (2015) Enabling visible-light water photooxidation by coordinative incorporation of Co(II/III) cocatalytic sites into organic-inorganic hybrids: quantum chemical modeling and photoelectrochemical performance, Journal of Coordination Chemistry, 68:17-18, 3317-3327, DOI: 10.1080/00958972.2015.1072624

To link to this article: http://dx.doi.org/10.1080/00958972.2015.1072624

Journal of Coordination Chemistry, 2015
Vol. 68, Nos. 17–18, 3317–3327, http://dx.doi.org/10.1080/00958972.2015.1072624

Enabling visible-light water photooxidation by coordinative incorporation of Co(II/III) cocatalytic sites into organic-inorganic hybrids: quantum chemical modeling and photoelectrochemical performance

OLEKSIY V. KHAVRYUCHENKO*†‡, LIDONG WANG§, DARIUSZ MITORAJ§, GILLES H. PESLHERBE‡¶ and RADIM BERANEK*§

†CompChem Group, Kyiv, Ukraine
‡Centre for Research in Molecular Modeling, Montréal, Canada
§Faculty of Chemistry and Biochemistry, Ruhr University Bochum, Bochum, Germany
¶Department of Chemistry and Biochemistry, Concordia University, Montréal, Canada

(*Received 21 March 2015; accepted 22 June 2015*)

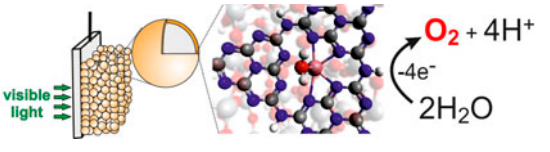

Coordinative incorporation of Co(II/III) cocatalytic sites into organic–inorganic hybrids of TiO_2 and "polyheptazine" (PH, poly(aminoimino)heptazine, melon, or "graphitic carbon nitride") has been investigated both by quantum chemical calculations and experimental techniques. Specifically, density-functional theory (DFT) calculations (PBE/def2-TZVPP) suggest that Co(II/III) and Zn(II) ions adsorb in nanocavities at the surface of the hybrid PH–TiO_2 cluster, a prediction which can be further confirmed experimentally by ^{15}N nuclear magnetic resonance in the case of the Zn complex. The absorption spectra of the complexes were characterized by time-dependent DFT calculations, suggesting a change of color upon Co ion binding which can in fact be observed with the naked eye. Hybrid TiO_2–PH photoelectrodes were impregnated with Co(II) ions from aqueous cobalt nitrate solutions. Optical absorption data suggest that Co(II) ions are predominantly present as single ions coordinated within the nitrogen cavities of TiO_2–PH, and any undesired blocking of light absorption is negligible. The cobalt-induced cocatalytic sites can efficiently couple to the holes photogenerated by visible light in TiO_2–PH, leading to complete oxidation of water to dioxygen. Our results indicate that coordinative incorporation of metal ions into well-designed surface sites in the light absorber is sufficient to drive complex multielectron transformations in artificial photosynthetic systems.

Keywords: Artificial photosynthesis; Water photooxidation; Photoanode; Cobalt; Oxygen evolution; Time-dependent density-functional theory; Hybrid materials

*Corresponding authors. Email: alexkhavr@gmail.com (O.V. Khavryuchenko); radim.beranek@rub.de (R. Beranek)
Dedicated to Professor Rudi van Eldik on the occasion of his 70th birthday.

1. Introduction

One of the most attractive strategies for maintaining the future supply of energy is the development of artificial photosynthetic systems capable of direct conversion of solar energy into the chemical energy stored in chemical bonds of molecular fuels [1, 2]. The most straightforward scenario of artificial photosynthesis would involve a solar-driven reduction of low-energy feedstock (e.g. protons and/or carbon dioxide) to high-energy solar fuels like hydrogen, hydrocarbons, or alcohols. In this context, it is important to realize that water is the only reducing agent which is abundant enough to serve as a sustainable source of electrons for such large-scale reductive transformations. However, oxidation of water to dioxygen is a highly complex process requiring a concerted proton-coupled transfer of four electrons out of two molecules of water [3]. Efficient oxidation of water to oxygen is therefore one of the major challenges in the development of artificial photosynthetic schemes. This is particularly true for solar water-splitting systems based on tandem photoelectrochemical cells which represent one of the most viable strategies for artificial photosynthesis, promising overall solar-to-hydrogen conversion efficiencies exceeding 25% [4–6]. Such tandem cells comprise spatially separated photocathodes and photoanodes driving the water reduction to hydrogen and water oxidation to oxygen, respectively. While photocathodes with impressive performance based, for example, on silicon have been reported recently [7, 8], a major challenge in the development of photoelectrochemical water-splitting cells is still the development of low-cost, efficient, and stable photoanodes. Such photoanodes must not only absorb strongly in the visible range (preferably under 2 eV, ~620 nm), but should also have the onset of photocurrent at potentials as low as ~ 0.2 V *versus* RHE (reversible hydrogen electrode) in order to match the current best-performing photocathodes. The latter criterion turns out to be very restrictive. It effectively rules out the use of passivated n-type silicon photoanodes, as well as the most widely investigated binary (e.g. WO_3 [9, 10] or α-Fe_2O_3 [11, 12]) and ternary (e.g. $BiVO_4$ [13]) metal oxides, since these all have their electronic quasi-Fermi level (i.e. the maximum negative photocurrent onset) at far too positive potentials. One possible strategy to overcome this problem is the use of alternative photochemical architectures in which the light-harvesting absorber (for example a dye) is able to inject electrons into a nanocrystalline layer of a wide-bandgap oxide with a relatively negative potential of the conduction band edge (e.g. for anatase TiO_2 at −0.15 V *versus* RHE [14, 15]). At the same time, the light absorber must be coupled to an oxygen evolution cocatalyst (e.g. colloidal IrO_x nanocrystals) [16–21] catalyzing the water oxidation by photogenerated holes. In such a way, the photoanode should be able to sustain water oxidation even at rather negative potentials near the quasi-Fermi level of the electron collector.

Following a similar concept, we have been recently developing photoanodes (figure 1) based on a hybrid absorber layer comprising of nanocrystalline TiO_2 and polyheptazine, "PH", more precisely poly(aminoimino)heptazine or melon, a CN_xH_y polymeric s-heptazine derivative, also often referred to as "graphitic carbon nitride" or "g-C_3N_4" in the literature [22–26]. A remarkable feature of PH is its very high thermal and chemical stability, making it a material of choice for photo(electro)catalytic applications [22, 27, 28]. Notably, PH forms a covalently grafted layer on TiO_2 with significant charge transfer, causing the optical absorption edge and the photocurrent response of TiO_2–PH hybrids to shift down to 2.3 eV (~540 nm), as compared to the corresponding bandgaps of both single components (~3.2 eV for anatase TiO_2; ~2.9 eV for PH) [22]. We have shown that porous TiO_2–PH photoanodes loaded with IrO_x or CoO_x acting as oxygen-evolving cocatalysts are capable of visible

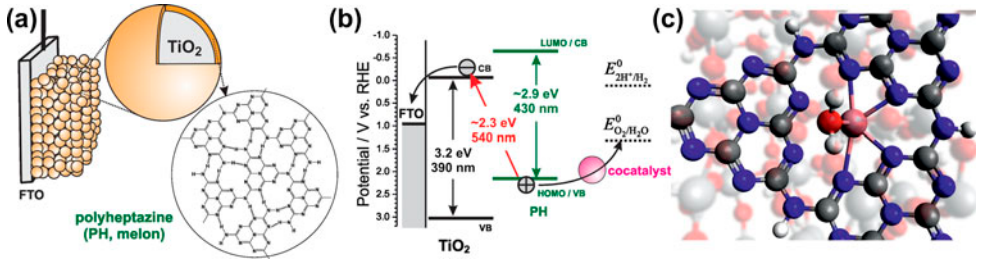

Figure 1. Metal-doped inorganic-organic hybrid photoelectrocatalytic system. (a) Concept of TiO_2–PH hybrid photoanodes. A nanocrystalline TiO_2 powder is pressed onto a transparent conductive FTO glass substrate, sintered, and subsequently modified at the surface with a thin layer of polyheptazine (PH, melon); (b) A simplified potential scheme illustrating the visible light photoactivity of TiO_2–polyheptazine hybrids based on direct optical excitation of an electron from the HOMO (valence band) of PH (with contributions of molecular orbitals formed upon interaction of PH with TiO_2 [23]) into the conduction band of TiO_2; (c) Schematic view of the PH sheets lying flat on the anatase surface and offering coordination sites for metal ions with one apical position available for the coordination of a water molecule.

light-driven oxygen evolution in aqueous electrolytes [22–26, 29]. The presence of a cocatalyst was absolutely necessary since *no* dioxygen evolution is observed at TiO_2–PH photoanodes without cocatalyst. In the absence of an efficient water oxidation cocatalyst, the photogenerated holes cannot oxidize water, accumulate in the surface PH layer, and eventually induce photodegradation of the hybrids by cleaving the bonds between PH and TiO_2 [29]. The deposition of the cocatalyst and the quality of its coupling to the TiO_2–PH light absorber is therefore of crucial importance. The cocatalyst deposition has been so far typically carried out by colloidal deposition or photoelectrochemically induced deposition and precipitation of IrO_x or CoO_x nanoparticles into the porous structure of the TiO_2–PH photoanode [22–26, 29]. One disadvantage of using metal oxide nanoparticles as cocatalysts is that the nanoparticles themselves can absorb light and thus block light absorption by the absorber [30]. An ideal oxygen evolution cocatalyst should be therefore transparent in the absorption range of the light absorber. This can be, for example, achieved by decreasing the cocatalyst size and thus breaking the well-developed band structure of relatively large metal oxide nanoparticles. In this context, it is important to realize that the PH sheets lying flat on the (dehydrated/dehydroxylated) anatase surface exhibit a twisted conformation of heptazine units with N atoms in the equatorial plane [23]. Such sites [figure 1(c)] look very promising for coordination of (single) metal ions to act as cocatalyst for water oxidation since it has one apical position available for coordination of a water molecule. To that effect, in this work, the adsorption of Co(II/III) and water onto an interfacial TiO_2–PH cluster has been modeled using density-functional theory (DFT). The concept has been further tested experimentally by investigating structural, optical and photoelectrocatalytic properties of hybrid TiO_2–PH photoanodes impregnated with small amounts of Co(II).

2. Methods

2.1. *Computational methodology and model design*

Quantum chemical calculations were performed within the framework of DFT, employing the Perdew, Burke, and Ernzerhof (PBE) functional [31, 32] that was used before for analogous

calculations [33, 34], together with Ahlrichs' triple-zeta split-valence basis set augmented by Coulomb fitting (def2-TZVPP) [35]. Molecular geometries were optimized for various relevant multiplicities to gradients of 5×10^{-6} Eh/bohr or less. Grimme's van der Waals empirical corrections were included in the calculation of energies [36]. Optical absorption spectra were obtained for optimized structures with conventional time-dependent DFT (TD-DFT). Up to 400 singlet excited states were included in the calculations to cover the whole visible spectrum range and intensities were evaluated from the electric transition dipole moments. The data were further convoluted with a Gaussian filter of halfwidth 500 cm^{-1} and converted to nm to obtain the spectra. The ORCA *ab initio*, DFT and semiempirical SCF-MO package [37] were used for all calculations.

In order to keep the DFT calculations manageable, the **Ti42** cluster used in previous work [23] could not be used and a more reasonable size had to be selected for the TiO_2 cluster. A $Ti_5O_{15}H_{10}$ cluster formed by a cycle of 5 TiO_4 tetrahedra was extracted from the **Ti42** cluster, as a representative fragment of the [1 0 1] anatase surface. Together with a cyclic trimer of heptazine, laying flat on the surface, it made up our TiO_2–PH mode system, denoted **Ti5M1** and shown in figure 2. One should note that the exact band structure in the calculated spectra has limited relevance due to the accuracy of the functional chosen and the reduced TiO_2 cluster size, and their interpretation of the results focuses on qualitative features such as the appearance of new bands in the visible range upon adsorption of transition metal ions.

2.2. *Experimental*

The preparation of hybrid TiO_2–PH photoelectrodes has been described before [23]. Briefly, an ethanolic suspension of TiO_2 was smeared on the cleaned fluorine-doped tin oxide (FTO) substrate, dried in air at 80 °C, pressed under the pressure of 200 kg cm^{-2} for 3 min, and calcined at 450 °C in air. To modify the surface of TiO_2 with polyheptazine, the electrodes were placed in a Schlenk tube connected via an adapter with a flask containing 1 g of urea and heated in a muffle oven at 425 °C for 30 min. ^{15}N-labeled urea (98%, Euriso-Top) has been used in the synthesis of samples for solid-state NMR.

The as-prepared hybrid electrodes were rinsed with water and dried under argon to remove the impurities and reaction by-products. TiO_2–PH–Co(II) and TiO_2–PH–Zn(II) samples were prepared by soaking the electrodes in $Co(NO_3)_2$ (0.1 M) and $Zn(NO_3)_2$ (0.1 M) aqueous solutions, respectively, for 24 h (if not stated otherwise). Powder TiO_2–PH–Co(II) and TiO_2–PH–Zn(II) samples were prepared similarly as above by impregnation, followed by washing with water (five times), and drying under vacuum at room temperature. For

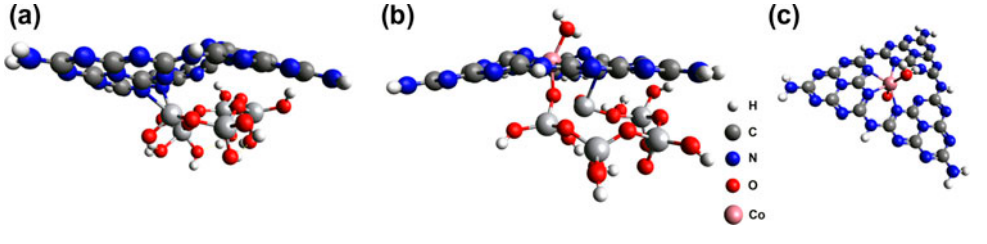

Figure 2. DFT-optimized geometries (PBE/def2-TZVPP) of the model **Ti5M1** systems. (a) singlet-state **Ti5M1**; (b) quintet-state **Ti5M1CoAq**$^{(3+)}$; (c) coordination of Co(III) in quintet-state **Ti5M1CoAq**$^{(3+)}$.

comparison, a physical mixture of TiO_2–PH and crystalline Co_3O_4 (Sigma Aldrich) was prepared by grinding. The amount of cobalt in powder samples was determined by ICP-OES (UNICAM 701) after chemical decomposition. The BET-specific surface area was measured by nitrogen physisorption in a Quantachrome Autosorb-1-MP setup.

UV/Vis diffuse reflectance spectra (DRS) were recorded on powder samples (25 mg) diluted in $BaSO_4$ (0.5 g) relative to the reflectance of a standard ($BaSO_4$) using a Perkin Elmer Lambda 650 UV–Vis spectrophotometer. The Kubelka–Munk function, $F(R_\infty) = (1 - R_\infty)^2/2R_\infty$, was used to determine the optical absorption properties of all samples, where R_∞ is the diffuse reflectance of the sample relative to the reflectance of a standard.

Solid state NMR spectra were recorded on a Bruker DSX 400-MHz spectrometer utilizing ZrO_2 rotors of 2.5-mm diameter at 293 K. Powders of the materials were ground and tightly pressed into the rotors. The rotors were sealed with a vespel cap and bottom. During measurement, the rotors were rotated at 20,000 Hz. The ^{15}N spectra were measured referenced to glycine and further recalculated and plotted using nitromethane as the reference.

The photoelectrocatalysis of water was carried out in a Na_2SO_4 (0.1 M, pH 6) electrolyte three-electrode system in a two-compartment cell. A platinum wire and an Ag/AgCl (3 M KCl) served as a counter electrode and reference electrode, respectively. A 150-W xenon lamp (Lot-Oriel) equipped with a 420-nm cut-off filter was used as the light source. The dissolved oxygen was measured using an OxySense 325i oxygen analyzer under an external bias of 0.5 V *versus* Ag/AgCl (i.e. 1.06 V *vs*. RHE). Prior to experiments the electrolyte was purged with argon.

3. Results and discussion

Both Co(II) and Co(III) can be adsorbed into nanocavities at the surface of the hybrid PH–TiO_2 cluster, with nitrogens in the equatorial plane and oxygens from the TiO_2 surface at the bottom (**Ti5M1CoAq**)[†] [figure 2(b) and (c)]. The Co ion has a highly distorted pseudo-C_s coordination sphere, with one axial position occupied by water (cf. table S1 [see online supplemental material at http://dx.doi.org/10.1080/00958972.2015.1072624] for structural parameters). One should emphasize that an "ideal" triangular model of PH was used in order to keep consistency with previous calculations, while recent experimental data [38–42] suggest that PH exhibits a more disordered combination of tri-*s*-triazine (heptazine) moieties. However, the adsorbed transition metals do not occupy the whole cavity of the PH, but rather "stick" to one of the corners. Therefore, the small distortion observed in the more realistic structure of PH should not affect the complexing ability of the PH on the titania surface.

The energies of the reactions are evaluated as the difference in electronic energies E(el):

$$\textbf{Ti5M1} + \left[\mathrm{Co(Aq)_6}\right]^{2+} \rightarrow \textbf{Ti5M1CoAq6}^{(2+)} \quad \Delta E_\mathrm{r}(\mathrm{el}) = -111.3\ \mathrm{kcal\,mol^{-1}}$$

and

$$\textbf{Ti5M1} + \left[\mathrm{Co(Aq)_6}\right]^{3+} \rightarrow \textbf{Ti5M1CoAq6}^{(3+)} \quad \Delta E_\mathrm{r}(\mathrm{el}) = -256.0\ \mathrm{kcal\,mol^{-1}}$$

(singlet state)[‡]

[†]**Aq** and numbers hereafter refer to the number of water molecules.

[‡]Initial and final systems ground state is singlet, but ΔE spin state change to quintet in the final state is only 3.5 kcal mol^{-1}.

The energy difference between the (quartet) Co(II) and (quintet)[†] Co(III) systems without additional adsorbed, H-bonded, water molecules (**Ti5M1CoAq**), E[Co(III)] − E[Co(II)], is 271.0 kcal mol^{-1}, while the difference for the aqua complex $[Co(Aq)_6]^{2+/3+}$ is 395.0 kcal mol^{-1} and that for $[Co(en)_3]^{2+/3+}$ is 286.3 kcal mol^{-1}. Therefore, complexation facilitates oxidation of Co(II)–Co(III), in accord with general rules known for amino complexes of Co. One should emphasize that entropy is not accounted for in this analysis, while it is known to have an important role in chelating processes.

In fact, the triplet **Ti5M1CoAq$^{(3+)}$** system lies only 2.4 kcal mol^{-1} and the singlet state only 1.0 kcal mol^{-1} higher in energy than the quintet state, the latter being a close ground state most probably due to the strongly distorted coordination polyhedron (as mentioned above). The axially-coordinated water is strongly H-bonded to the neighboring N of the heptazine moiety ($d_{N–H}$ ~ 1.80 Å for Co^{2+} and ~2.00 Å for Co^{3+}) in **Ti5M1CoAq**. When a cluster of H-bonded water molecules is attached to the coordinated water (**Ti5M1CoAq6**), one or two of these molecules are H-bonded to the N of heptazine. This leads to stabilization of the singlet state in comparison to the quintet by 3.5 kcal mol^{-1}, so taking into account the relative accuracy of the calculations, it is hard to ascribe with high certainty the exact spin state of the ground state. A proton transfer from water to heptazine can occur [$\Delta E^{\dagger}$(el) ~ 10.7 kcal mol^{-1} for Co(II) in the quartet state and 6.3 kcal mol^{-1} for Co(III) in the singlet state, figure S1 (i)]. Although the reaction is endothermic [ΔE_r(el) = 1.4 and 4.5 kcal mol^{-1}, respectively], it is kinetically feasible and may further facilitate oxidation of water.

Modeling of the hybrid TiO_2–PH–Co(II/III)–water system demonstrates that both Co(II) and Co(III) ions can adsorb in the nanocavities at the surface of the model hybrid PH–TiO_2 cluster, with the water molecule in axial position activated by the presence of electron-donating groups of the neighboring heptazines. Importantly, the Zn(II) ion can occupy the same cavity and form a surface complex with analogous structure (cf. table S1 for structural parameters), and one can note that structural parameters are quite close to those of the Co(II) complex. This will prove useful later since the structure of the Zn complex is probed by ^{15}N NMR.

We now turn our attention to changes in the electronic absorption spectra of the model TiO_2–PH system upon adsorption of transition metal ions. First, two reference systems were considered, namely the $[Co(en)_3]^{3+}$ complex and the **Ti5M1** cluster, both known to have yellow color. As one can see in figure 3, the absorption peaks of both systems lie below 500 nm, in accord with experimental data. Addition of Zn(II) does not change the calculated spectrum noticeably, which is expected due to lack of *d-d* electronic transitions in the Zn ion (and also indicates no charge transfer from the metal to the ligand). However, the spectra of the TiO_2–PH–Co(III) (singlet-state **Ti5M1CoAq**) and TiO_2–PH–Co(II) (quartet-state **Ti5M1CoAq**) model systems are very rich and cover almost the whole visible range, which is probably explained by the distorted geometry of the coordination center. One should note that the exact position of the absorption peaks can differ from center to center due to the amorphous nature of both the TiO_2 surface and the TiO_2–PH composite. From figure 3, the observed color of the sample should be close to dark blue or even gray, especially if both oxidation states of Co are present at the surface. This means that the

[†]As discussed below, singlet, triplet and quintet states for such system are pseudo-spin-degenerate, so spin-conservation rule might be more important in this case than the overall thermodynamics of the reaction including possible spin cross-over.

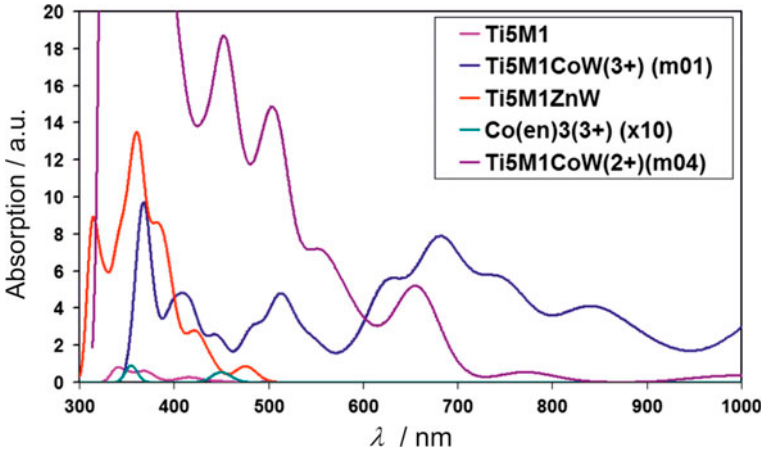

Figure 3. TD-DFT simulated absorption spectra. The broadening parameter σ is 500 cm^{-1} (Intensities normalized to those of the quartet-state **Ti5M1CoAq**$^{(2+)}$ spectrum, intensities of the $[Co(en)_3]^{3+}$ spectrum are magnified by a factor of 10 for clarity).

adsorption of both Co(II) and Co(III) on the TiO_2–PH interface might lead to an observable change of color of the sample.

In order to investigate the incorporation of Co(II) into the TiO_2–PH hybrids experimentally, we have impregnated TiO_2–PH with Co(II) from aqueous cobalt nitrate solutions. With the purpose of probing the possibility of metal ion complexation in PH by ^{15}N solid-state NMR spectroscopy, we impregnated TiO_2–PH also with Zn(II) ions which are diamagnetic. The complexation of Zn(II) in the nitrogen cavities of PH is expected to lead to deshielding of the nuclei and, thus, to a weak-field shift of the peaks. Indeed, the ^{15}N NMR spectrum (figure 4) of TiO_2–PH–Zn(II) exhibits a weak-field shift by 45 ppm as compared to pristine TiO_2–PH, which is in line with the literature data for other Zn

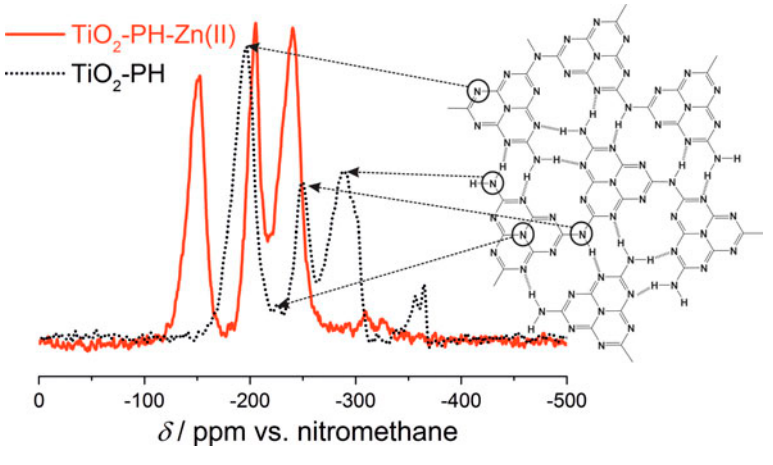

Figure 4. ^{15}N solid-state NMR spectra of bare TiO_2–PH powder and TiO_2–PH impregnated with Zn(II). The peak assignment is based on Ref. [38].

complexes [43, 44]. It can be assumed that Co(II/III) ions potentially enter the same cavity as Zn(II), and coordinate in the same manner (as shown by DFT calculations).

As expected, the amount of cobalt ions adsorbed on TiO_2–PH–Co(II) is very small (0.24 ± 0.05 wt%). Given the specific surface area (BET) of TiO_2–PH–Co(II) of 56.4 $m^2\ g^{-1}$, this loading translates into a surface density of 1 Co(II) ion per 2.3 nm^2. This very low surface density suggests that most of the Co(II) ions are present as single Co(II) sites, without substantial aggregation into cobalt hydroxide/oxide clusters. As we were also unable to detect any cobalt oxide phase by Raman spectroscopy, in order to further corroborate this conclusion, we have investigated the optical absorption spectra of TiO_2–PH–Co(II) by diffuse reflectance spectroscopy. For comparison, we prepared also a physical mixture of TiO_2–PH with Co_3O_4 powder (0.24 wt%). The normalized spectra (figure 5) show that the incorporation of Co does not lead to any significant shift of the fundamental absorption edge of TiO_2–PH. In other words, the light absorption in TiO_2–PH–Co(II) will still be dominated by the electronic transitions in TiO_2–PH. On the other hand, the very weak tail absorption in the low-energy range ($\lambda > 520$ nm) is enhanced, which is in line with our DFT calculations (figure 3). In stark contrast, the physical mixture TiO_2–PH–Co_3O_4 shows a completely distinct absorption feature peaking at 730 nm, a typical absorption fingerprint of Co_3O_4 particles [45]. Though the presence of other phases like, for example, very small cobalt hydroxide clusters cannot be completely ruled out, this clear difference in absorption spectra supports our assumption that the adsorption of Co(II) in TiO_2–PH–Co(II) leads mainly to isolated Co(II) sites in the cavities within PH.

Finally, we have investigated the performance of TiO_2–PH–Co(II) photoanodes in the photoelectrochemical oxidation of water. Figure 6 shows the photocurrent response and oxygen evolution of TiO_2–PH–Co(II) under visible light ($\lambda > 420$ nm) irradiation at 1.06 V *versus* RHE. We note that at relatively low bias potentials (~0.2 V *vs*. RHE), photocurrents were detectable but very small due to the fast back electron transfer (primary recombination) [29]. A higher bias potential was therefore applied in order to obtain larger photocurrents and detectable amounts of oxygen. By using the *visible light only* we effectively "switch off" the intrinsic light absorption by TiO_2, so that *all* photocurrent response is

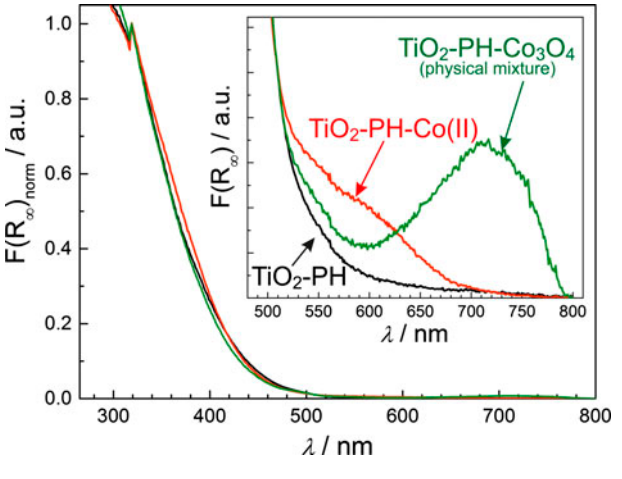

Figure 5. Normalized DRS of TiO_2–PH, TiO_2–PH–Co(II), and a physical mixture of TiO_2–PH with a small amount (0.24 wt%) of commercial Co_3O_4.

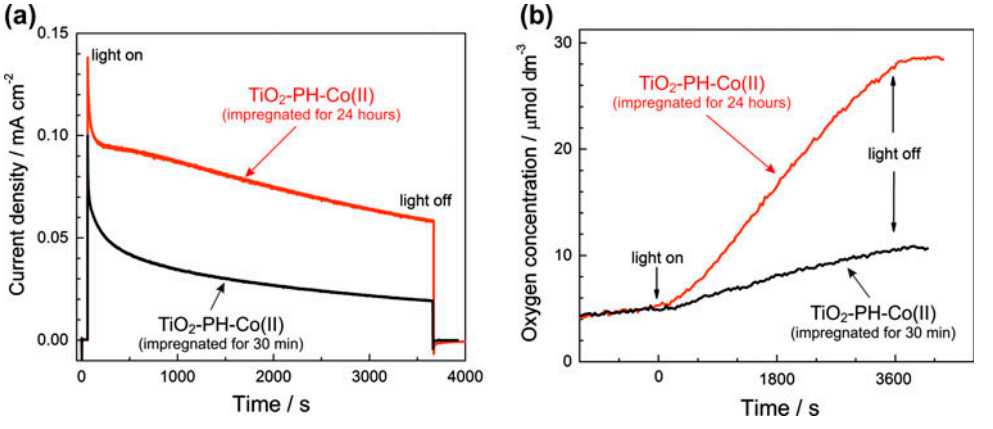

Figure 6. Photoelectrocatalytic properties of TiO_2–PH–Co photoanodes. (a) Photocurrents and (b) oxygen evolution measured during irradiation by polychromatic *visible* light (Xenon solar simulator, cut-off filter $\lambda > 420$ nm) at 1.06 V *vs*. RHE in a Na_2SO_4 (0.1 M) electrolyte.

chiefly due to the visible light absorption by the TiO_2–PH hybrid. The photocurrent transients suggest a typical behavior of TiO_2–PH photoelectrodes characterized by fast increase of photocurrents after switching on the light, followed by an immediate drop of photocurrents due to accumulation of holes in the PH layer [23, 25, 29]. These accumulated holes either oxidize water or contribute to recombination and photocorrosion of the TiO_2–PH light absorber (by breaking the bonds between TiO_2 and PH). The latter effect leads to continuous decrease of photocurrent during prolonged irradiation [figure 6(a)]. However, a significant portion of holes is long-lived enough to induce complete water photooxidation to dioxygen during irradiation by visible light [figure 6(b)]. The faradaic efficiency (current-to-oxygen conversion efficiency) of oxygen evolution was 38.6% for a photoelectrode impregnated by Co(II) for 24 h. This value is relatively high taking into account the fact that faradaic efficiencies in porous dye-sensitized photoanodes for water oxidation are often around 20% [16]. Interestingly, when the impregnation time was shortened to 30 min, both the photocurrent and oxygen evolution rate decreased, resulting in a faradaic efficiency drop to 25.1%. These results indicate that relatively longer soaking times are needed for cobalt ions to penetrate the porous structure of the TiO_2–PH photoelectrode. No oxygen evolution was observed at pristine TiO_2–PH photoelectrodes [23, 25, 29]. It should be also noted that slight darkening of the TiO_2–PH–Co(II) layer was observed with the naked eye during the photoelectrocatalytic reaction. After photoelectrocatalysis, the darkening slowly faded within a few days. We assume that this darkening is related to the oxidation of Co(II) to Co (III) during the photoelectrocatalytic action, as confirmed by the DFT-calculated energy of Co(II/III) complex oxidation (see above).

4. Conclusion

Modeling of the hybrid TiO_2–PH–Co(II/III)–water systems demonstrates that both Co(II) and Co(III) ions can adsorb in nanocavities at the surface of the hybrid PH–TiO_2 cluster, which has the heptazine nitrogens in the equatorial plane and O from the TiO_2 surface lying

at the bottom. The Co ion has a highly distorted pseudo-C_s-symmetry coordination sphere, with one axial position occupied by a water molecule, which is activated by the presence of electron-donating groups of the neighboring heptazines. Experimental results show that hybrid TiO_2–PH photoelectrodes can be successfully impregnated with Co(II) ions from aqueous cobalt nitrate solutions. The spectroscopic data suggest that Co(II) ions are predominantly present as single ions coordinated within the nitrogen cavities of TiO_2–PH. Such cocatalytic sites do not block light absorption by TiO_2–PH but can efficiently couple to the holes photogenerated by visible light in TiO_2–PH, leading to complete oxidation of water to dioxygen. In general, our results show that even a very small amount of metal ions coordinatively incorporated into well-designed surface sites in the light absorber is sufficient to drive complex multielectron transformations which are crucial for efficient operation of artificial photosynthetic systems.

Acknowledgments

Computational resources were provided by the Centre for Research in Molecular Modeling (CERMM) and Calcul Québec. G.H.P. is a Concordia University Research Fellow. We thank the Sachtleben company for providing Hombikat UV 100. The support of the Center for Electrochemical Sciences (CES) is gratefully acknowledged.

Disclosure statement

No potential conflict of interest was reported by the authors.

Funding

This work was funded in part by the Ministére de l'éducation, du Loisir et du Sport du Québec and Concordia University. R.B., L.W. and D.M. are thankful for financial support by the MIWFT-NRW within the project "Anorganische Nanomaterialien für Anwendungen in der Photokatalyse: Wasseraufbereitung und Wasserstoffgewinnung" and by the EU-FP7 Grant "4G-PHOTOCAT" [grant number 309636].

References

[1] N.S. Lewis, D.G. Nocera. *Proc. Natl. Acad. Sci. USA*, **103**, 15729 (2006).
[2] T.A. Faunce, W. Lubitz, A.W. Rutherford, D. MacFarlane, G.F. Moore, P. Yang, D.G. Nocera, T.A. Moore, D.H. Gregory, S. Fukuzumi, K.B. Yoon, F.A. Armstrong, M.R. Wasielewski, S. Styring. *Energy Environ. Sci.*, **6**, 695 (2013).
[3] H. Dau, C. Limberg, T. Reier, M. Risch, S. Roggan, P. Strasser. *ChemCatChem*, **2**, 724 (2010).
[4] M.G. Walter, E.L. Warren, J.R. McKone, S.W. Boettcher, Q. Mi, E.A. Santori, N.S. Lewis. *Chem. Rev.*, **110**, 6446 (2010).
[5] A.J. Nozik. *Appl. Phys. Lett.*, **29**, 150 (1976).
[6] S. Hu, C. Xiang, S. Haussener, A.D. Berger, N.S. Lewis. *Energy Environ. Sci.*, **6**, 2984 (2013).
[7] S.W. Boettcher, E.L. Warren, M.C. Putnam, E.A. Santori, D. Turner-Evans, M.D. Kelzenberg, M.G. Walter, J.R. McKone, B.S. Brunschwig, H.A. Atwater, N.S. Lewis. *J. Am. Chem. Soc.*, **133**, 1216 (2011).
[8] B. Seger, T. Pedersen, A.B. Laursen, P.C.K. Vesborg, O. Hansen, I. Chorkendorff. *J. Am. Chem. Soc.*, **135**, 1057 (2013).
[9] R. Solarska, A. Królikowska, J. Augustyński. *Angew. Chem., Int. Ed.*, **49**, 7980 (2010).
[10] V.S. Vidyarthi, M. Hofmann, A. Savan, K. Sliozberg, D. König, R. Beranek, W. Schuhmann, A. Ludwig. *Int. J. Hydrogen Energy*, **36**, 4724 (2011).

[11] A. Kay, I. Cesar, M. Grätzel. *J. Am. Chem. Soc.*, **128**, 15714 (2006).
[12] K.G. Upul Wijayantha, S. Saremi-Yarahmadi, L.M. Peter. Phys. Chem. Chem. Phys., **13**, 5264 (2011).
[13] F.F. Abdi, L. Han, A.H.M. Smets, M. Zeman, B. Dam, R. van de Krol. *Nat. Commun.*, **4**, 2195 (2013).
[14] L. Kavan, M. Grätzel, S.E. Gilbert, C. Klemenz, H.J. Scheel. *J. Am. Chem. Soc.*, **118**, 6716 (1996).
[15] R. Beranek. *Adv. Phys. Chem.*, 786759, (2011). doi:10.1155/2011/786759.
[16] W.J. Youngblood, S.-H.A. Lee, Y. Kobayashi, E.A. Hernandez-Pagan, P.G. Hoertz, T.A. Moore, A.L. Moore, D. Gust, T.E. Mallouk. *J. Am. Chem. Soc.*, **131**, 926 (2009).
[17] W.J. Youngblood, S.-H.A. Lee, K. Maeda, T.E. Mallouk. *Acc. Chem. Res.*, **42**, 1966 (2009).
[18] G.F. Moore, J.D. Blakemore, R.L. Milot, J.F. Hull, H. Song, L. Cai, C.A. Schmuttenmaer, R.H. Crabtree, G.W. Brudvig. *Energy Environ. Sci.*, **4**, 2389 (2011).
[19] Y. Zhao, J.R. Swierk, J.D. Megiatto, B. Sherman, W.J. Youngblood, D. Qin, D.M. Lentz, A.L. Moore, T.A. Moore, D. Gust, T.E. Mallouk. *Proc. Natl. Acad. Sci. USA*, **109**, 15612 (2012).
[20] J.R. Swierk, T.E. Mallouk. *Chem. Soc. Rev.*, **42**, 2357 (2013).
[21] J.R. Swierk, N.S. McCool, T.P. Saunders, G.D. Barber, M.E. Strayer, N.M. Vargas-Barbosa, T.E. Mallouk. *J. Phys. Chem. C*, **118**, 17046 (2014).
[22] M. Bledowski, L. Wang, A. Ramakrishnan, O.V. Khavryuchenko, V.D. Khavryuchenko, P.C. Ricci, J. Strunk, T. Cremer, C. Kolbeck, R. Beranek. *Phys. Chem. Chem. Phys.*, **13**, 21511 (2011).
[23] M. Bledowski, L. Wang, A. Ramakrishnan, A. Bétard, O.V. Khavryuchenko, R. Beranek. *ChemPhysChem*, **13**, 3018 (2012).
[24] M. Bledowski, L. Wang, A. Ramakrishnan, R. Beranek. *J. Mater. Res.*, **28**, 411 (2013).
[25] L. Wang, M. Bledowski, A. Ramakrishnan, D. König, A. Ludwig, R. Beranek. *J. Electrochem. Soc.*, **159**, H616 (2012).
[26] B. Mei, H. Byford, M. Bledowski, L. Wang, J. Strunk, M. Muhler, R. Beranek. *Sol. Energy Mater. Sol. Cells*, **117**, 48 (2013).
[27] X. Wang, K. Maeda, A. Thomas, K. Takanabe, G. Xin, J.M. Carlsson, K. Domen, M. Antonietti. *Nat. Mater.*, **8**, 76 (2009).
[28] D.J. Martin, P.J.T. Reardon, S.J.A. Moniz, J. Tang. *J. Am. Chem. Soc.*, **136**, 12568 (2014).
[29] M. Bledowski, L. Wang, S. Neubert, D. Mitoraj, R. Beranek. *J. Phys. Chem. C*, **118**, 18951 (2014).
[30] L. Trotochaud, T.J. Mills, S.W. Boettcher. *J. Phys. Chem. Lett.*, **4**, 931 (2013).
[31] J.P. Perdew, K. Burke, M. Ernzerhof. *Phys. Rev. Lett.*, **77**, 3865 (1996).
[32] J.P. Perdew, K. Burke, M. Ernzerhof. *Phys. Rev. Lett.*, **78**, 1396 (1997).
[33] C.J. Cramer, D.G. Truhlar. *Phys. Chem. Chem. Phys.*, **11**, 10757 (2009).
[34] R. Sánchez-de-Armas, M.A. San-Miguel, J. Oviedo, A. Márquez, J.F. Sanz. *Phys. Chem. Chem. Phys.*, **13**, 1506 (2011).
[35] F. Weigend, R. Ahlrichs. *Phys. Chem. Chem. Phys.*, **7**, 3297 (2005).
[36] S. Grimme. *J. Comput. Chem.*, **27**, 1787 (2006).
[37] F. Neese. *Wiley Interdiscip. Rev. Comput. Mol. Sci.*, **2**, 73 (2012).
[38] B.V. Lotsch, M. Döblinger, J. Sehnert, L. Seyfarth, J. Senker, O. Oeckler, W. Schnick. *Chem.-Eur. J.*, **13**, 4969 (2007).
[39] Y. Wang, X. Wang, M. Antonietti. *Angew. Chem., Int. Ed.*, **51**, 68 (2012).
[40] Y. Zheng, J. Liu, J. Liang, M. Jaroniec, S.Z. Qiao. *Energy Environ. Sci.*, **5**, 6717 (2012).
[41] A. Schwarzer, T. Saplinova, E. Kroke. *Coord. Chem. Rev.*, **257**, 2032 (2013).
[42] P. Niu, L.-C. Yin, Y.-Q. Yang, G. Liu, H.-M. Cheng. *Adv. Mater.*, **26**, 8046 (2014).
[43] T.E. Wood, B. Berno, C.S. Beshara, A. Thompson. *J. Org. Chem.*, **71**, 2964 (2006).
[44] R. Marek, A. Lycka, E. Kolehmainen, E. Sievanen, J. Tousek. *Curr. Org. Chem.*, **11**, 1154 (2007).
[45] T. He, D. Chen, X. Jiao, Y. Wang, Y. Duan. *Chem. Mater.*, **17**, 4023 (2005).